



OPEN

Bifunctional catalytic effect of Mo₂C/oxide interface on multi-layer graphene growth

Seda Kizir¹✉, Wesley T. E. van den Beld¹, Bart Schurink¹, Robbert W. E. van de Kruijs¹, Jos P. H. Benschop^{1,2} & Fred Bijkerk¹

The role of the Mo₂C/oxide interface on multi-layer graphene (MLG) nucleation during a chemical vapor deposition (CVD) process is investigated. During the CVD process, MLG growth is only observed in the presence of a Mo₂C/SiO₂ interface, indicating that the chemical reactions occurring at this interface trigger the nucleation of MLG. The chemical reaction pathway is explained in four steps as (1) creation of H radicals, (2) reduction of the oxide surface, (3) formation of C–C bonds at O–H sites, and (4) expansion of graphitic domains on the Mo₂C catalyst. Different Mo₂C/oxide interfaces are investigated, with varying affinity for reduction in a hydrogen environment. The results demonstrate a catalyst/oxide bifunctionality on MLG nucleation, comprising of CH₄ dehydrogenation by Mo₂C and initial C–C bond formation at the oxide interface.

Graphene is a two-dimensional material with unique properties such as high carrier mobility¹, high strength², and high optical transparency³, which is advantageous for application areas such as transistors⁴, solar cells⁵, sensors⁶, and batteries⁷. Chemical vapor deposition (CVD) is currently the most promising method to synthesize large scale graphene for industrial applications^{8,9}. Mo₂C, from the transition metal carbide (TMC) family, is a leading candidate as a catalyst for uniform mono/multi-layer graphene synthesis due to its noble metal like catalytic activity, low cost, and high thermal stability^{10–12}.

In our previous work, the growth of multi-layer graphene (MLG) was linked to the presence of pinholes in Mo₂C thin films¹³. Such pinholes could expose the underlying oxide, which may play an important role in the graphene synthesis process. It is known from the field of catalysis that underlying oxide, commonly known as the “support layer”, can actively participate in catalytic reactions^{14–16}. As an example, the influence of the support layer on carbon nanotube (CNT) synthesis is widely studied^{17–19}, and it is found that the oxide interface causes initial CNT nucleation^{18,20}. It is stated that ordered carbon formation on oxide is triggered by hydroxide and oxygen species^{18,20}, which can be potentially important for MLG synthesis. Furthermore, Mo₂C is a catalyst that shows different catalytic activity depending on the oxide under-layer (support) used^{21,22}. Mo₂C in combination with ZSM-5 zeolite supports causes aromatization of CH₄, whereas this is not the case for only Mo₂C or ZSM-5 separately²³. This shows that both the catalyst and neighboring oxide can play a role in graphene synthesis, which to our knowledge has not yet been investigated.

In this study, we will demonstrate that the interface between pinhole-free Mo₂C and SiO₂ is triggering MLG nucleation upon the CVD process. We will introduce a model for explaining the MLG nucleation by catalyst/oxide bi-functionality. This model is based on the complementary role of MoC_x (x = 0–0.5) for CH₄ dehydrogenation and SiO₂ for C–C bond formation after reduction with hydrogen. We will test this model by performing the CVD process in absence of hydrogen gas, as well as using different oxide (TiO₂, Al₂O₃, MgO) interfaces, in which we expect a dependence of MLG nucleation on the oxide reducibility. The outcome of this study shows that the catalyst-oxide interface interaction is crucial for understanding the MLG synthesis on Mo₂C thin films.

Methods

In this section, the MLG synthesis process will be explained in three parts. In the first part, the thin film deposition process flow of Mo catalysts on Si/SiO₂ substrates will be given. This process is known to result in pinhole-free Mo₂C, which does not yield MLG growth upon subsequent CVD processing¹³. In the second part, the deposition/patterning of oxides will be explained in order to create an interface which is expected to play a role

¹Industrial Focus Group XUV Optics, MESA + Institute of Nanotechnology, University of Twente, 7522 NB Enschede, The Netherlands. ²ASML Netherlands B.V., 5504 DR Veldhoven, The Netherlands. ✉email: s.kizir@utwente.nl

Material	Deposition pressure (E-4 mbar)	Ar (sscm)	O ₂ (sscm)	Current (A)	Voltage (V)	Target name (4 in.), supplier purity (%)
Mo	8.5	30	0	1	378	Mo, Robeko, 99.95
SiO ₂	7.8	20	20	0.25	306	Si, Sindhauser, 99.9999
TiO ₂	7.2	18	18	1	570	Ti, Robeko, 99.5
Al ₂ O ₃	4.2	11	11	1.5	386	Al, Sindhauser, 99.99
MgO	7.9	20	20	1	172	Mg, Sindhauser, 99.95

Table 1. Overview of the used sputtering parameters.

in MLG synthesis. In the final part, the applied CVD process for MLG growth, and characterization methods for analyzing synthesized MLG, will be described.

To remove possible surface contamination and the native oxide layer on top, *p*-type (100) single side polished silicon wafers are cleaned with ozone steam and HF, sequentially. To prevent Mo₂C/Si interdiffusion, a 300 nm thermal SiO₂ layer is grown on top of Si, by means of a dry oxidation process at 1100 °C. Directly before the sputtering process, the samples are cleaned with HNO₃ to remove any organic contaminants on the sample surface. For the majority of samples, a Mo layer is deposited onto the SiO₂ layer using magnetron sputtering, resulting in a pinhole-free Mo₂C layer upon the CVD process described in ref 13. A nominal Mo layer thickness of 70 nm was used for all samples, because in separate experiments it was shown that thinner Mo layers (with pinholes) result in graphene layers with significant higher D/G ratios. This is explained by the strong reduction of the Mo crystallite size for thinner layers, which is expected to correlate to the formation of more pinholes and therefore significantly higher MLG nucleation density. In addition, 'standard' MLG thickness for 70 nm Mo layer (with pinholes) is around 11 nm corresponding to 32 layers, according to low energy ion scattering (LEIS) measurements (not shown here). After Mo deposition, a specific oxide top layer was deposited onto each sample using reactive sputtering. All sputter depositions are carried out in the same UHV deposition chamber, with a target to substrate distance of 300 mm and a base pressure of 10⁻⁸ mbar, using the conditions given in Table 1.

To test the impact of an exposed Mo/oxide interface on MLG growth, several procedures were developed based on optical UV lithography and including various wet etching/lift off steps, yielding a patterned oxide layer with lines and line spaces ranging from 1 to 10 micron, with length scales chosen similar to typical graphene domain sizes observed in previous studies. For creating an exposed Mo/SiO₂ interface, two methods were developed. One method involves patterning the SiO₂ layer before the deposition of Mo, as schematically shown in Fig. 1a. To fabricate a line step significantly higher than the thickness of the Mo layer, the thermal SiO₂ layer is wet etched by buffered hydrofluoric acid (BHF) for 2 min resulting in a step of 150 nm. A Mo layer is then deposited at an off-normal angle, inducing a "shadow" in the deposited area on one side of the steps (shown by a black circle, Fig. 1a), leading to an exposed interface between Mo and SiO₂. Another method to create an exposed Mo/SiO₂ interface involves a lift-off process. Here, a 'lift-off resist' (LOR) and a top regular photoresist are deposited on top of the Mo/SiO₂/Si layers. Subsequently, the LOR/photoresist is patterned upon UV exposure, a final 10 nm SiO₂ layer is deposited, and the lift-off step is performed (as shown in Fig. 1b). In order to study and compare the influence of various other Mo/oxide interfaces on MLG nucleation and growth, a third structure was developed, where a 10 nm oxide layer (either SiO₂, TiO₂, Al₂O₃, or MgO) is deposited on top of Mo/SiO₂/Si, as shown in Fig. 1c. To create an interface, the BHF wet etching process flow is used for oxide patterning, to avoid difficulties of removing lift-off resist for different oxides.

After fabrication of samples with exposed Mo/oxide interfaces, a CVD process is applied to all samples using a cold wall reactor system in presence of CH₄, Ar and, H₂ gases at 1000 °C for 35 min, using the same parameters from our previous study¹³. To test the role of hydrogen in the MLG growth process, additional experiments were done where the same CVD process was applied, but without H₂.

To characterize the structure of CVD deposited carbon, Raman measurements are performed, using a WITec alpha 300 system with a 0.9 NA objective and a 532 nm wavelength laser. The power of the laser is adjusted to 1 mW to avoid damage to graphene. The Raman spectra are recorded over a 10 by 10 micro meter area, and averaged for 9 spectra. I_d/I_g ratios of graphene layers are obtained by processing of the Raman data with a MATLAB script using Lorentian peak fitting and normalization. The surface topography and elemental contrast imaging are carried out using a Zeiss MERLIN HR-SEM system with a voltage of 1.4 kV for improved surface sensitivity and in addition an EsB detector is used to make the nano-scale composition visible.

Results and discussion

In our earlier work¹³, it is shown that the nucleation and growth (or absence thereof) of MLG on Mo₂C was strongly related to the presence (or absence) of pinholes in Mo₂C. From this observation, we hypothesize that the Mo₂C/SiO₂ interface can play an important, bifunctional, role by catalyzing different reactions for MLG growth. To test our hypothesis, in this section we investigate the role of the Mo₂C/SiO₂ interface in MLG growth on pinhole-free Mo₂C.

Effect of Mo₂C/SiO₂ interface on MLG nucleation. To create a system where within one sample both exposed and unexposed Mo₂C/SiO₂ interfaces are present, the structure as defined in Fig. 1a was prepared and subsequently exposed to the CVD process.

In Fig. 2a, c the cross-section SEM images of the left and right side of the step after the CVD process is presented, showing (a) a Mo₂C layer with an exposed Mo₂C/SiO₂ interface on the left side of the step, and (c) a

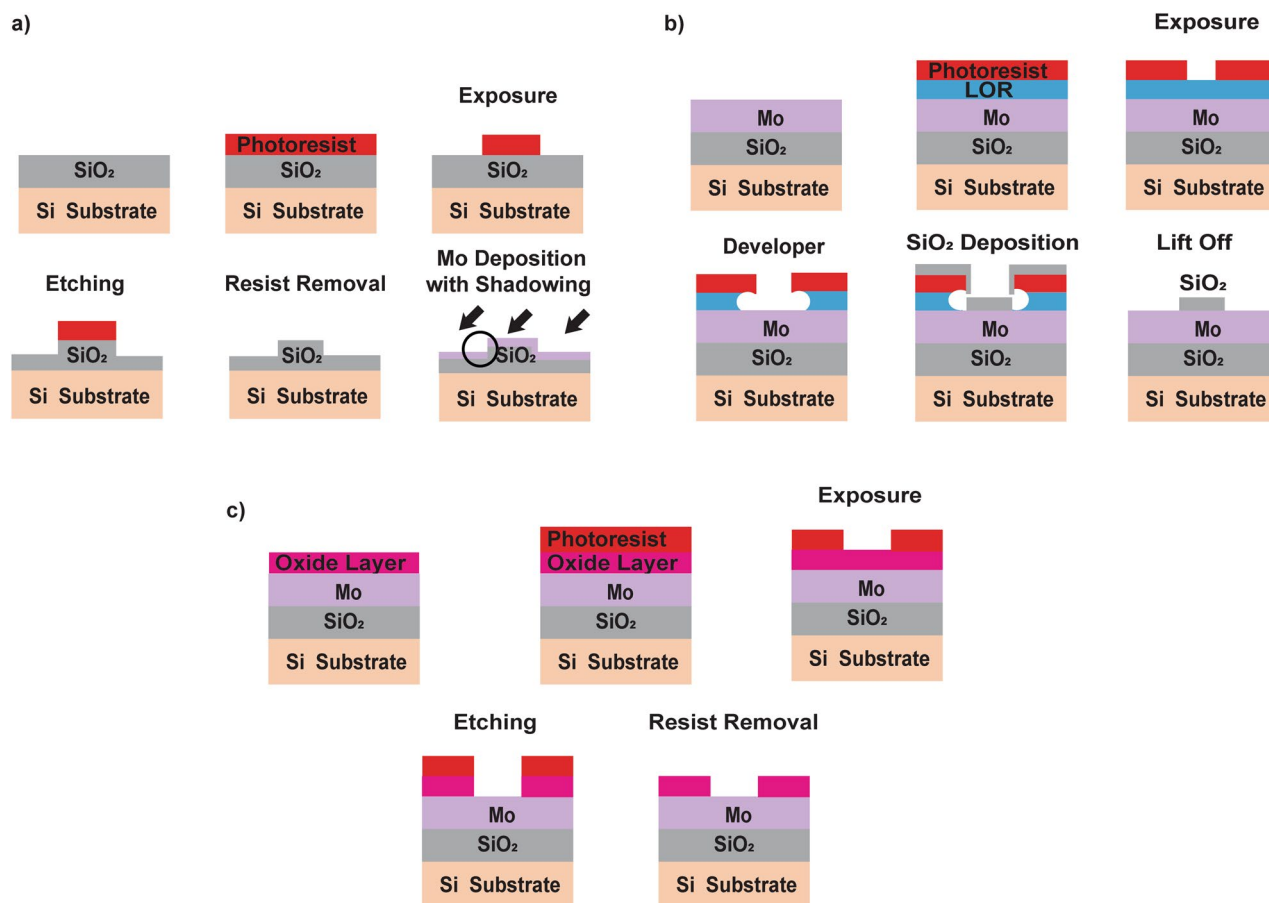


Figure 1. Schematic process of (a) SiO₂ step fabrication via wet etching process and shadowed deposition of Mo, (b) lift off patterning of SiO₂ lines on Mo layer, (c) wet etching patterning process for SiO₂, TiO₂, Al₂O₃ and MgO.

continuous Mo₂C layer on the right side of the step. Based on our hypothesis, MLG growth is expected where the Mo/SiO₂ interface is exposed to the CVD process, as sketched in Fig. 2b. In Fig. 2d, the elemental contrast mode of SEM indeed confirms the presence of carbonaceous species (dark colour) centred on the exposed interface. The Raman spectrum is shown in Fig. 2e, confirming the characteristic peaks of MLG which are known as D, G, 2D peaks. This clearly suggest that MLG growth is initiated at the exposed Mo₂C/SiO₂ interface.

In the following section, we will propose a model explaining the MLG nucleation mechanism taking place exclusively at the exposed Mo₂C/SiO₂ interface.

MLG nucleation model. According to the d-band model, Mo has a strong interaction towards adsorbates such as CH₄ leading to formation of a molybdenum carbide²⁴, which is also known to occur upon the CVD process used for MLG synthesis^{10,11}. In-situ formed Mo₂C is generally considered as a catalyst for the MLG synthesis process, since it has noble metal like catalytic activity due to its modified band structure by compound formation^{10,11}.

In this section, a chemical reaction pathway will be proposed for MLG nucleation on Mo₂C, with particular emphasis on the role of the exposed Mo₂C/SiO₂ interface, as indicated in Fig. 3.

Step 1: Formation of radicals. The first step of MLG nucleation is the adsorption and subsequent dehydrogenation of CH₄ on the Mo surface. Mo has a high reactivity towards dehydrogenation of CH₄ due to its d-band structure, resulting in formation of C* and H* radicals.

Step 2: Diffusion of radicals. The reaction pathway continues with the diffusion of C* and H* radicals, formed in the previous step. C* species diffuse into the Mo layer to form a stable carbide structure via Mo–C chemical bond formation^{10,11}. Although some of the H radicals can diffuse into the Mo layer from grain boundary defects, this is expected to be minimal due to its low hydrogen permeability^{25,26}. A part of the H* species is expected to diffuse over the Mo₂C surface and onto the SiO₂ surface, known as ‘Hydrogen spillover’²⁷ (Fig. 3, Step 2). These diffused atomic H* species can cause a reduction of SiO₂, especially at temperatures as high as 1000 °C^{27,28} causing activation of surface O–H sites.

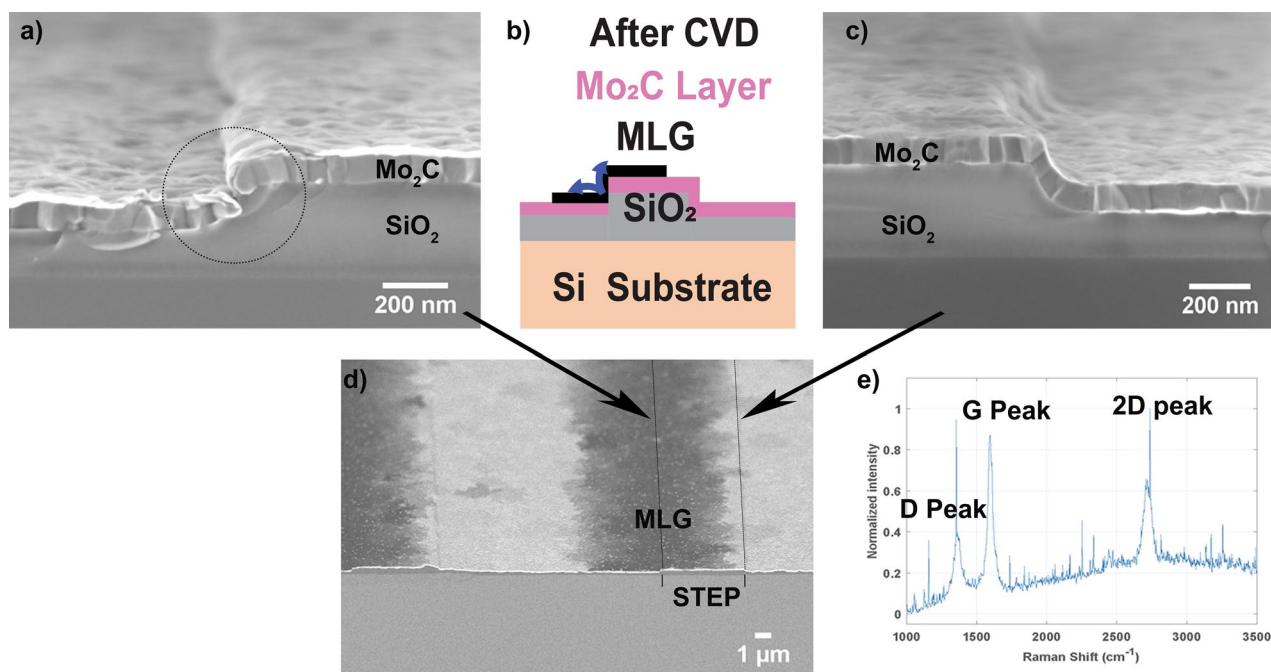


Figure 2. (b) Schematic image after CVD process is represented, where left side shows the MLG deposition from interface. SEM image after CVD process showing the cross-section from top view (a) Mo₂C/SiO₂ interface with dotted circle (left), (c) step fully covered with only Mo₂C (Right) and (d) full view of the same step with elemental contrast mode imaging, in which MLG growth is shown around the left side of step with black contrast, and no graphene growth around right side of step with light contrast. (e) The Raman spectra after CVD process shows the deposition of MLG layers due to presence of D, G and 2D peaks.

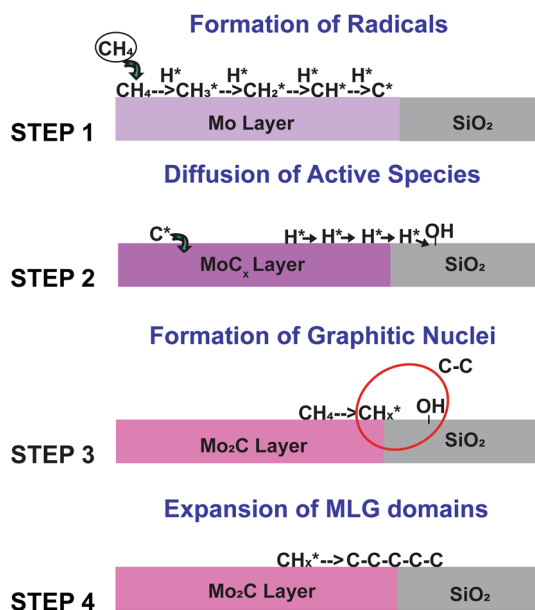


Figure 3. Schematic view of MLG nucleation model is explained in four steps.

Step 3: Formation of graphitic nuclei. Once the Mo₂C catalyst is formed, the generation of CH_x^{*} radicals will continue on the catalyst surface via dehydrogenation of CH₄²³. These CH_x^{*} radicals can be adsorbed chemically on SiO₂ surfaces at the interface through O–H sites, created in the previous step. This results in graphitic carbon formation via C–C coupling (Fig. 3, Step 3), which is a commonly known mechanism for graphene nucleation on SiO₂ substrates^{29–31}.

Step 4: Expansion of MLG domains. Once graphitic nuclei form at the interface between Mo₂C and SiO₂, MLG domains expand dominantly onto the Mo₂C surface since the graphene growth rate on SiO₂ is generally orders of magnitude slower^{32,33}.

In summary, the MLG nucleation model proposed here is effectively driven by the Mo₂C/SiO₂ bi-functionality, where the oxide layer promotes the initial C–C bond formation whereas Mo₂C causes CH₄ dehydrogenation leading to the creation of radicals and expansion of MLG domains on its surface. Similar phenomena have also been reported for CNTs, where the oxide interface caused initial nucleation of CNTs and further growth continued on the catalyst by attachment of C species to the edge of the graphitic nuclei¹⁸. In the following section, the critical assumptions of the model based on support layer bi-functionality (steps 2 and 3) will be validated.

Hydrogen spillover impact on MLG growth. In this section, we aim to study the importance of hydrogen spillover on the MLG growth process. In the MLG nucleation model in STEP 1, the expected source of the spillover H radicals is either the dehydrogenation of CH₄ (CH₄ → CH₃ → CH₂ → CH → C), formed upon the transition of Mo to Mo₂C, or cracking of H₂ (H₂ → H* + H*) during the CVD process. To investigate the role of H₂ in the creation of OH sites (and thereby being responsible for the MLG nucleation), experiments were carried out with and without hydrogen gas.

To fabricate a sharp Mo/SiO₂ interface, two identical samples are prepared using lithography and lift-off processes, (See more details on the experimental section, Fig. 1b). The first sample is used as a reference in which our standard CVD process is applied (with Ar, H₂, and CH₄ gasses), whereas, for the second one, the CVD process is applied in absence of H₂ gas, as shown schematically in Fig. 4a, b. The arrows indicate the transport (“spillover”) from Mo₂C towards SiO₂.

In Fig. 4c, d, the Raman spectra after the CVD process are shown. For both samples, D, G, and 2D peaks typical for MLG growth are observed³⁴, suggesting that CH₄ dehydrogenation upon carbide formation creates sufficient H radicals for MLG nucleation via spillover (MLG nucleation model, step 2). While the G and 2D peaks exhibit similar I_{2d}/I_g ratios for both samples, the I_d/I_g ratio is reduced significantly in absence of H₂ gas in the CVD process (Fig. 4e). A lower I_d/I_g ratio in the MLG growth process without H₂ gas indicates the formation of larger domains, which suggests fewer nucleation sites³⁵.

Reduction of the support layer. A critical step in the proposed model is the creation of OH sites through reduction of the oxide layer by H*. To investigate the importance of the oxide reduction step, we compare samples with different oxides (SiO₂, TiO₂, Al₂O₃, MgO), chosen based on their difference in reducibility. Specifically, the order of reducibility in an atomic hydrogen environment is expected to be SiO₂ > TiO₂ > Al₂O₃ > MgO, with energies – 135.568 > – 120.763 > – 53.733 > – 15.632 kJ/mol O₂²⁸ with respect to their Gibbs free energy at 1000 K.

For interface formation, the oxide line patterns were created on top in order not to affect Mo₂C crystallinity. A patterned surface with Mo/oxide interfaces was created for all samples using lithography and BHF wet etching (for more details, see experimental section Fig. 1c). Except for the sample with the MgO layer, all samples are patterned with a high yield. We believe that the sample with MgO continued to etch in the rinsing water after the BHF etching step, therefore only local patterns on sample could be analyzed.

In Fig. 5a–c, the Raman spectra after the CVD process are shown. Raman spectra indicate that sample with SiO₂ lines showed strong MLG growth, whereas sample with TiO₂ lines showed patchy growth and no growth is observed for the sample with Al₂O₃ lines. MLG growth is observed for SiO₂ lines with the presence of D, G, and 2D peaks, showing similar spectra when compared to the lift-off patterned sample. The smaller appearance of the 2D peak for TiO₂ suggests patchy deposition. No appearance of the 2D peak for Al₂O₃ indicates that there is no deposition of graphene. The local MgO patterns could not be traced back using Raman microscopy and thus no Raman spectra could be recorded. The Raman results clearly indicate that the reducibility of the oxide has a strong impact on graphene growth.

In order to semi-quantify the amount of carbonaceous species, the samples are analyzed simultaneously with the topography/elemental contrast mode of SEM, resulting in side-by-side images (Fig. 5d–g). Here, the elemental contrast mode shows the oxides and the carbonaceous species with darker contrast caused by their relatively low atomic number compared to the Mo-containing catalyst. The highest amount of carbon deposition is observed for SiO₂ with dark contrast in between the lines. A smaller amount of carbonaceous deposition is observed on the edges of TiO₂ lines. On Al₂O₃ and MgO samples, the carbon species are not observed. These SEM images correlate well with the observations from Raman, regarding the relation between oxide reducibility and graphene growth. These results therefore support our MLG nucleation model in which oxide reduction is a key step in creating OH sites required for triggering MLG nucleation.

The observed difference between SiO₂ and TiO₂ illustrated in Fig. 5a, b also suggests that the chemical reactivity for these oxides towards graphitization might be different, which is caused by a difference in the number of reactive sites and/or its strength^{36,37}. In addition, the generation of intermediate volatile (reaction) products such as Si–O³⁸, and, Si–H³⁹, may lead to accumulation of graphitic carbon, similar to the graphene growth on SiC substrates^{39–41}.

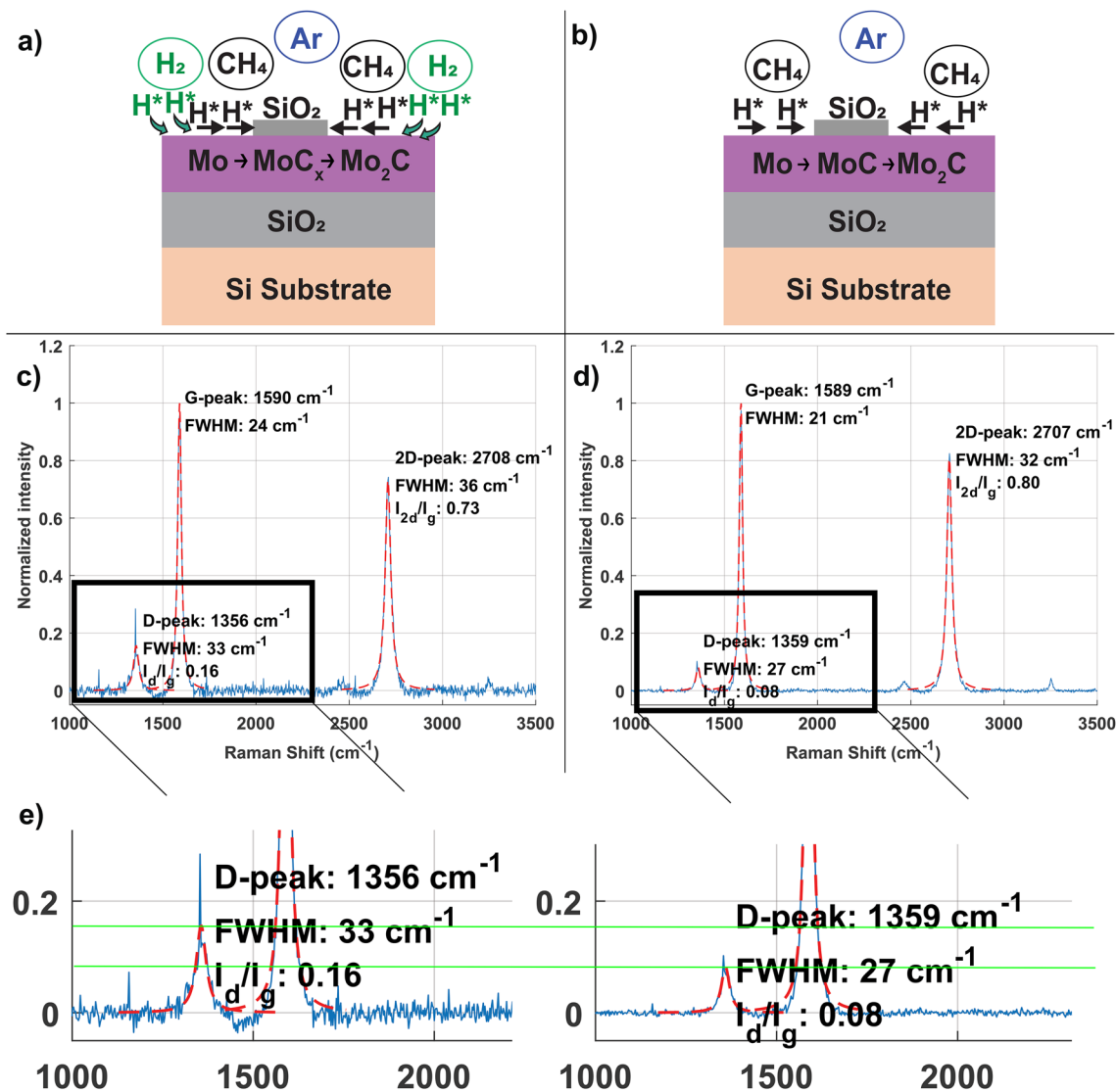


Figure 4. Schematic images showing the H spill-over during the CVD process for (a) standard CVD process, (b) CVD process in absence of external H₂ gas. Corresponding Raman spectra depicting the MLG growth for both samples given as (c) sample with H₂ gas in standard CVD process and (d) without, showing a difference in D peak. (e) Raman spectra zoomed in to D-peak region, comparing the I_d/I_g ratios of the two samples, where for clarification a guide to eye was added (green line).

Conclusions

In this report, the active role of the Mo₂C/oxide interface on MLG nucleation is shown experimentally. A MLG nucleation model is proposed based on sequential chemical reactions, namely the formation of H species via CH₄ dehydrogenation/H₂ cracking, the migration of H species on the SiO₂ surface (spillover), the reduction of the SiO₂ surface, the activation of C–C bonds at O–H sites (as discussed in STEP 3- MLG nucleation model), and the expansion of graphitic domains onto Mo₂C. It was shown that the dehydrogenation of CH₄ is already sufficient to supply the H* species required for oxide reduction, whereas additional H* through cracking of H₂ likely only increases the number of nucleation sites and reduces domain sizes. The Mo₂C/oxide bi-functionality is further studied by using different oxide layers with varying reducibility. Increased reducibility leads to increased graphene growth, confirming the importance of the role of oxide reduction in the proposed model. The results shown here contribute to unraveling the role of the catalyst/support interactions that take place in graphene synthesis, as such the bifunctional catalytic effect of the oxide under layer. This could be also relevant for other catalyst/support combinations, yet more research is needed to deeper understand bifunctional chemical reactions at the atomistic level.

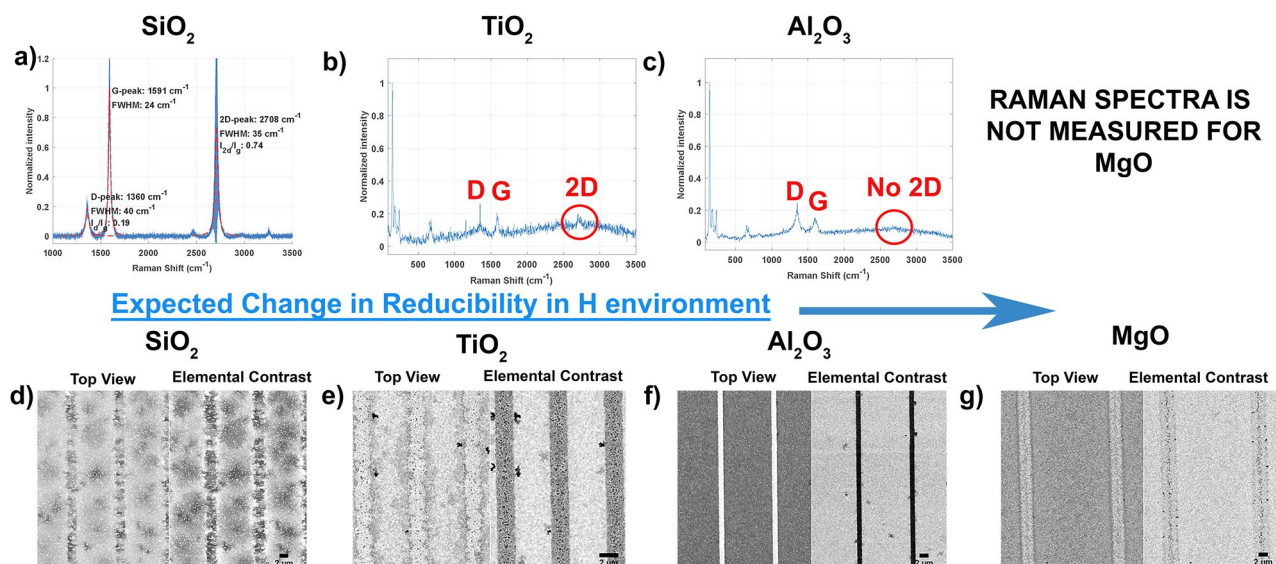


Figure 5. Reduction in the H environment follows the trend as $\text{SiO}_2 > \text{TiO}_2 > \text{Al}_2\text{O}_3 > \text{MgO}$ ³¹. **(d)** Schematic view shows the presence of O–H bonds with respect to reduction on oxide surface. Raman results are given, indicating MLG growth for SiO_2 patterned sample **(a)**, local growth with the appearance of small 2D peak for TiO_2 patterned sample **(b)** and no growth for Al_2O_3 patterned sample **(c)**. SEM results after CVD process is given with **(d)** SiO_2 , **(e)** TiO_2 , **(f)** Al_2O_3 , **(g)** MgO lines on Mo_2C , showing the C species with dark contrast in elemental contrast mode images.

Received: 17 May 2021; Accepted: 12 July 2021

Published online: 28 July 2021

References

- Banszerus, L. *et al.* Ultrahigh-mobility graphene devices from chemical vapor deposition on reusable copper. *Sci. Adv.* **1**, 1–7 (2015).
- Lee, C. *et al.* Measurement of the elastic properties and intrinsic strength of monolayer. *Graphene* **321**, 385–388 (2016).
- Sheehy, D. E. & Schmalian, J. Optical transparency of graphene as determined by the fine-structure constant. *Phys. Rev. B Condens. Matter Mater. Phys.* **80**, 19 (2009).
- Reddy, D., Register, L. F., Carpenter, G. D. & Banerjee, S. K. Graphene field-effect transistors. *J. Phys. D. Appl. Phys.* **45**, 1 (2011).
- Miao, X. *et al.* High efficiency graphene solar cells by chemical doping. *Nano Lett.* **12**, 6, 2745–2750 (2012).
- Yang, T., Zhao, X., He, Y. & Zhu, H. *Graphene-based sensors. Graphene, 157-174* (Elsevier Inc., 2017).
- Guo, P., Song, H. & Chen, X. Electrochemical performance of graphene nanosheets as anode material for lithium-ion batteries. *Electrochem. Commun.* **11**, 1320–1324 (2009).
- Chen, X., Zhang, L. & Chen, S. Large area CVD growth of graphene. *Synth. Met.* **210**, 95–108 (2015).
- Zhang, Y., Zhang, L. & Zhou, C. Review of chemical vapor deposition of graphene and related applications. *Acc. Chem. Res.* **46**, 2329–2339 (2013).
- Zou, Z., Fu, L., Song, X., Zhang, Y. & Liu, Z. Carbide-forming groups IVB–VIB metals: A new territory in the periodic table for CVD growth of graphene. *Nano Lett.* **14**, 3832–3839 (2014).
- Grachova, Y., Vollebregt, S., Lacaite, A. L. & Sarro, P. M. High quality wafer-scale CVD graphene on molybdenum thin film for sensing application. *Procedia Eng.* **87**, 1501–1504 (2014).
- Wu, Y. *et al.* Synthesis of large-area graphene on molybdenum foils by chemical vapor deposition. *Carbon N. Y.* **50**, 5226–5231 (2012).
- Kizir, S. *et al.* The role of pinhole structures in Mo thin films on multi-layer graphene synthesis. *J. Phys. Mater.* <https://doi.org/10.1088/2515-7639/ab6fd1> (2020).
- Ober, P., Rogg, S. & Hess, C. Direct evidence for active support participation in oxide catalysis: Multiple operando spectroscopy of VO_x/ceria . *ACS Catal.* **10**, 2999–3008 (2020).
- Schubert, M. M. *et al.* CO oxidation over supported gold catalysts—“Inert” and ‘active’ support materials and their role for the oxygen supply during reaction. *J. Catal.* **197**, 113–122 (2001).
- Jeness, G. R. & Schmidt, J. R. Unraveling the role of metal-support interactions in heterogeneous catalysis: Oxygenate selectivity in Fischer–Tropsch synthesis. *ACS Catal.* **3**, 2881–2890 (2013).
- Magrez, A. *et al.* Striking influence of the catalyst support and its acid-base properties: New insight into the growth mechanism of carbon nanotubes. *ACS Nano* **5**, 3428–3437 (2011).
- Rümmeli, M. H. *et al.* Oxide-driven carbon nanotube growth in supported catalyst CVD. *J. Am. Chem. Soc.* **129**, 15772–15773 (2007).
- Oliveira, H. A., Franceschini, D. F. & Passos, F. B. Support effect on carbon nanotube growth by methane chemical vapor deposition on cobalt catalysts. *J. Braz. Chem. Soc.* **23**, 868–879 (2012).
- Rümmeli, M. H. *et al.* On the graphitization nature of oxides for the formation of carbon nanostructures. *Chem. Mater.* **19**, 4105–4107 (2007).
- Pasupulety, N., Al-Zahrani, A. A., Daous, M. A., Driss, H. & Petrov, L. A. Studies on molybdenum carbide supported HZSM-5 (Si/Al = 23, 30, 50 and 80) catalysts for aromatization of methane. *Arab. J. Chem.* **13**, 5199–5207 (2020).
- Liu, X. & Smith, K. J. Acidity and deactivation of $\text{Mo}_2\text{C}/\text{HY}$ catalysts used for the hydrogenation and ring opening of naphthalene. *Appl. Catal. A Gen.* **335**, 230–240 (2008).

23. Ren, J. *et al.* Density functional theory study into the adsorption of CO₂, H and CH_x (x = 0–3) as well as C₂H₄ on α-Mo₂C(0 0 0 1). *Surf. Sci.* **600**, 2329–2337 (2006).
24. Liu, P. & Rodriguez, J. A. Catalytic properties of molybdenum carbide, nitride and phosphide: A theoretical study. *Catal. Lett.* **91**, 247–252 (2003).
25. Ogorodnikova, O. V. Ion-driven deuterium retention in high-Z metals. *J. Nucl. Mater.* **390–391**, 651–654 (2009).
26. Nemanič, V. Hydrogen permeation barriers: Basic requirements, materials selection, deposition methods, and quality evaluation. *Nucl. Mater. Energy* **19**, 451–457 (2019).
27. Prins, R. Hydrogen spillover. Facts and fiction. *Chem. Rev.* **112**, 2714–2738 (2012).
28. Sabat, K. C., Rajput, P., Paramguru, R. K., Bhoi, B. & Mishra, B. K. Reduction of oxide minerals by hydrogen plasma: An overview. *Plasma Chem. Plasma Process.* **34**, 1–23 (2014).
29. Liang, T., Luan, C., Chen, H. & Xu, M. Exploring oxygen in graphene chemical vapor deposition synthesis. *Nanoscale* **9**, 3719–3735 (2017).
30. Chen, J. *et al.* Oxygen-aided synthesis of polycrystalline graphene on silicon dioxide substrates. *J. Am. Chem. Soc.* **133**, 17548–17551 (2011).
31. Muñoz, R. *et al.* Direct synthesis of graphene on silicon oxide by low temperature plasma enhanced chemical vapor deposition. *Nanoscale* **10**, 12779–12787 (2018).
32. Zhou, L. *et al.* Ultrafast growth of uniform multi-layer graphene films directly on silicon dioxide substrates. *Nanomaterials* **9**, 1–11 (2019).
33. Xu, X. *et al.* Ultrafast growth of single-crystal graphene assisted by a continuous oxygen supply. *Nat. Nanotechnol.* **11**, 930–935 (2016).
34. Niilisk, A., Kozlova, J., Alles, H., Aarik, J. & Sammelselg, V. Raman characterization of stacking in multi-layer graphene grown on Ni. *Carbon N. Y.* **98**, 658–665 (2016).
35. Lee, D. *et al.* Significant enhancement of the electrical transport properties of graphene films by controlling the surface roughness of Cu foils before and during chemical vapor deposition. *Nanoscale* **6**, 12943–12951 (2014).
36. Solymosi, F. & Széchenyi, A. Aromatization of n-butane and 1-butene over supported Mo₂C catalyst. *J. Catal.* **223**, 221–231 (2004).
37. Karge, H. G. & Boldingh, E. P. In-situ IR investigation of coke formation on dealuminated mordenite catalysts. *Catal. Today* **3**, 53–63 (1988).
38. Akazawa, H., Takahashi, J., Utsumi, Y., Kawashima, I. & Urisu, T. Role of hydrogen in synchrotron-radiation-stimulated evaporation of amorphous SiO₂ and microcrystalline Si. *Appl. Phys. Lett.* **60**, 974–976 (1992).
39. Dagher, R. *et al.* A comparative study of graphene growth on SiC by hydrogen-CVD or Si sublimation through thermodynamic simulations. *CrystEngComm* **20**, 3702–3710 (2018).
40. Mishra, N., Boeckl, J., Motta, N. & Iacopi, F. Graphene growth on silicon carbide: A review. *Phys. Status Solidi Appl. Mater. Sci.* **213**, 2277–2289 (2016).
41. Powers, J. M. & Somorjai, G. A. The surface oxidation of alpha-silicon carbide by O₂ from 300 to 1373 K. *Surf. Sci.* **244**(1–2), 39–50 (1991).

Acknowledgements

This work is supported by the Technology Foundation STW which is part of the Netherlands Organization for Scientific Research (NWO), (Top sector High Tech Systems and Materials Project 15357). We acknowledge the funding from NWO and ASML (Veldhoven). The authors thank the Industrial Focus Group XUV Optics at the University of Twente, for facilitating the research, and ASML, Carl Zeiss SMT, and Malvern Analytical, for miscellaneous contributions. Also, the authors would like to thank Mark Smithers (MESA+ Nanolab) for his help with SEM measurements.

Author contributions

S.K.: Methodology, Investigation, Writing—original draft. W.T.E van den B.: Methodology, Investigation, Supervision, Writing—review and editing. B.S.: Methodology, Writing—review and editing. R.W.E van de K.: Methodology, Supervision, Writing—review and editing. J.P.H.B.: Supervision, Writing—review and editing. F.B.: Supervision, Funding acquisition, Writing—review and editing.

Competing interests

The authors declare no competing interests.

Additional information

Correspondence and requests for materials should be addressed to S.K.

Reprints and permissions information is available at www.nature.com/reprints.

Publisher's note Springer Nature remains neutral with regard to jurisdictional claims in published maps and institutional affiliations.



Open Access This article is licensed under a Creative Commons Attribution 4.0 International License, which permits use, sharing, adaptation, distribution and reproduction in any medium or format, as long as you give appropriate credit to the original author(s) and the source, provide a link to the Creative Commons licence, and indicate if changes were made. The images or other third party material in this article are included in the article's Creative Commons licence, unless indicated otherwise in a credit line to the material. If material is not included in the article's Creative Commons licence and your intended use is not permitted by statutory regulation or exceeds the permitted use, you will need to obtain permission directly from the copyright holder. To view a copy of this licence, visit <http://creativecommons.org/licenses/by/4.0/>.

© The Author(s) 2021